IET Microwaves, Antennas & Propagation

Research Article

IET Journals
The Institution of Engineering and Technology

Design of tunable microstrip diplexer with reconfigurable filtering characteristics based on dual-mode square loop resonators

ISSN 1751-8725
Received on 18th December 2019
Revised 28th May 2020
Accepted on 16th July 2020
E-First on 7th September 2020
doi: 10.1049/iet-map.2019.1133
www.ietdl.org

Ali Kursad Gorur[1] ✉, Engin Dogan[2], Ceyhun Karpuz[3], Adnan Gorur[2]

[1]*Department of Electrical and Electronics Engineering, Nevsehir Haci Bektas Veli University, Nevsehir, Turkey*
[2]*Department of Electrical and Electronics Engineering, Nigde Omer Halisdemir University, Nigde, Turkey*
[3]*Department of Electrical and Electronics Engineering, Pamukkale University, Denizli, Turkey*
✉ *E-mail: akursadgorur@hotmail.com*

Abstract: A novel compact microstrip diplexer with tunable centre frequencies and reconfigurable filtering characteristics at both channels is presented. The designed diplexer is constructed by coupling two dual-mode square loop resonators (DMSLRs) having different electrical lengths. The DMSLRs are investigated by virtue of the coupled line analysis to evaluate the resonance frequencies, transmission zeros and out-band insertion loss level more conveniently. Centre frequencies of both channels can be independently tuned by the varactor diodes utilised instead of perturbation and reference capacitances. Depending on the specialised values of perturbation and reference capacitances, filtering characteristics of both channels can be reconfigured in terms of transmission zeros. The designed diplexer was fabricated and tested for the experimental studies and the measurements were obtained in a good agreement with the predicted results. Tuning ranges of the measured centre frequency in the first channel are between 1.23 and 1.43 and 1.35 and 1.64 GHz for the filtering characteristics with right- and left-side transmission zeros, respectively. In the second channel, they are 2.07–2.31 and 2.14–2.51 GHz for the filtering characteristics with real- and imaginary-axis transmission zeros, respectively. Isolation between two channels has been obtained better than 22 dB.

1 Introduction

Depending on the fast developments in wireless communication systems, multi-function filters and multiplexers stand out since they can operate in multiple frequencies. Such circuits can also allow different filtering characteristics due to the occurrence of transmission zeros and poles. Therefore, tunable multiplexers are one of the most important components among multi-function multiplexers. Although there are many ways to implement microwave filters and multiplexers, microstrip structures are the mostly applied practical solutions since it is easier to obtain multiple passbands or channels within a compact size and low cost.

To date, researchers have designed and analysed many types of multiplexers by means of different approaches such as coupled lines [1, 2], stepped-impedance resonator [3] and ring resonators [4, 5]. A multi-channel diplexer, triplexer or quadruplexer structures have gained significance due to their multi-function features [6–9]. Tunable diplexers have also been studied for utilisation in multi-function communication systems since they can serve in different frequencies at both channels. A microstrip diplexer with tunable bandwidth was designed by using dual-mode ring resonators with varactor diodes [10]. Independently switchable passbands for a multi-channel diplexer were introduced by dual-mode stub-loaded resonators [11]. As well as tunable bandwidth and switchable passbands, centre frequency tuning mechanisms have also been introduced in several studies [11–22]. In [12], two bandpass channels with tunable centre frequencies were obtained by using varactor-tuned stepped impedance resonators. Another compact-sized diplexer design with tunable centre frequency was presented by using stub-loaded dual-mode resonators [13]. Tunability has been achieved by varactor diodes connected to the open-ended stubs [13]. Folded open-loop ring resonators were used to design a tunable diplexer [14]. Although the channels exhibit good performance in terms of losses and isolation, the tuning ranges for both channels are narrow. Schottky diodes are also used in tunable diplexers instead of varactor diodes. In [15], a tunable diplexer with a high tuning range and the reconfigurable matching network was introduced by using Schottky diodes. A common resonator approach was presented to design a three-pole tunable diplexer with flexible tuning characteristics. Another tunable three-pole diplexer with multiple transmission zeros was designed by using quarter and half-wavelength resonators [16]. For the common resonator approach, a diplexer with separately designable channels was also introduced in [17]. Moreover, a diplexer with tunable centre frequency but fixed fractional bandwidth (FBW) was proposed using stepped-impedance dual-mode resonators without the need for matching circuitry [18]. Tunable diplexers with constant absolute bandwidths (ABWs) were also designed based on tri-mode resonators and coupled resonators in [19, 20], respectively. In [21], the substrate-integrated waveguide structure was used to design diplexers with tunable transmission zeros, but the transmission zeros cannot be tuned electronically. However, diplexers with reconfigurable filtering characteristics at both channels have not yet been investigated and reported in the literature.

The main goal of this paper is to design a tunable microstrip diplexer with independently reconfigurable channels for GPS and 4G-LTE technologies. For this purpose, by keeping any channel fixed, electronically reconfigurable filtering characteristics at the other channel with respect to the existence of transmission zeros are desired. To our knowledge, a microstrip diplexer having tunable centre frequencies and reconfigurable filtering responses based on dual-mode square loop resonators (DMSLRs) is proposed for the first time. The proposed diplexer is constructed by combining two dual-mode bandpass filters at different centre frequencies. The DMSLRs are coupled to input and output (I/O) ports by folded feeding lines. They are investigated by coupled line theory under even and odd mode excitations in order to obtain the resonance frequencies, transmission zeros and also out-band insertion loss level. Varactor diodes are used to represent patch capacitive elements, as in the conventional DMSLRs [23, 24]. Due to the capacitance changes of the varactor diodes, even and odd modes of the DMSLRs can be independently tuned. Hence, both channels of the proposed diplexer can be electronically tuned by bias voltages feeding the varactor diodes. The designed diplexer

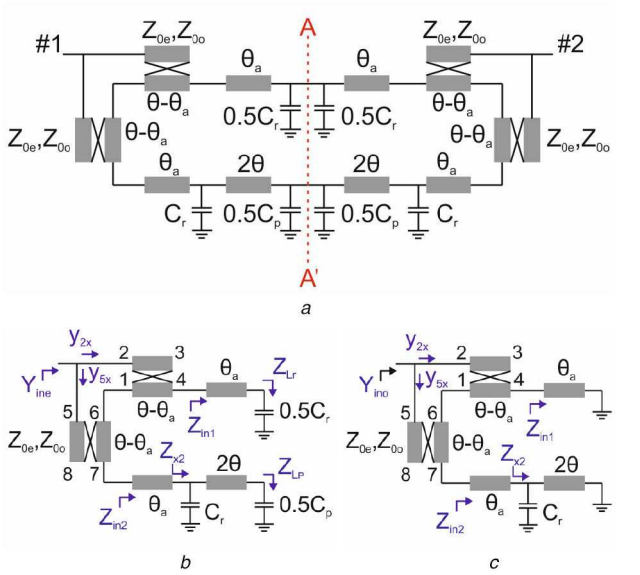

Fig. 1 *Equivalent circuits*
(a) Equivalent circuit for a coupled DMSLR, ***(b)*** Even mode half circuit model, ***(c)*** Odd mode half circuit model

was fabricated to demonstrate the verification of the proposed approach.

This paper is organised as follows. Section 2 describes the analysis of a DMSLR based on coupled line theory. Alternative coupling configurations including asymmetric couplings between the feeding line and DMSLR and folded feeding lines are also explained here. Section 3 contains the design methodology of the proposed tunable diplexer and simulation results. Fabricated circuit and measured results are given in Section 4.

2 Resonator analysis

2.1 Even–odd mode analysis

An equivalent circuit model for a DMSLR coupled to feeding lines of I/O ports is shown in Fig. 1*a*. In Fig. 1*a*, the electrical lengths are represented with θ and θ_a, where $\theta-\theta_a$ corresponds to the electrical length of the coupled section (Z_{0e} and Z_{0o} are even and odd mode characteristic impedances). The reference and perturbation capacitors are also represented with C_r and C_p, respectively [24]. In order to analyse the circuit, even and odd mode, half circuits can be obtained by placing magnetic and electric wall to the symmetry axis (AA′), respectively. Thus, the symmetry axis must be open and short-circuited for even and odd mode, as illustrated in Figs. 1*b* and *c*, respectively. From the even mode half circuit shown in Fig. 1*b*, it can be observed that, $V_1 = V_6$, $V_2 = V_5$, $I_1 = -I_6$, $I_3 = 0$, $I_8 = 0$, $V_4 = -I_4 Z_{in1}$ and $V_7 = -I_7 Z_{in2}$. These conditions are also valid for the odd mode half circuit depicted in Fig. 1*c*. It is obvious that the even and odd mode half circuits have an only difference in terms of the reference and perturbation capacitances in the symmetry axis. In Fig. 1*b*, Z_{in1} and Z_{in2} are the input impedances seen from the coupled sections for the upper and lower paths, respectively, and can be expressed as follows:

$$Z_{in1} = Z_1 \frac{Z_{Lr} + jZ_1 \tan\theta_a}{Z_1 + jZ_{Lr}\tan\theta_a} \tag{1a}$$

$$Z_{in2} = Z_1 \frac{Z_{x2} + jZ_1 \tan\theta_a}{Z_1 + jZ_{x2}\tan\theta_a} \tag{1b}$$

$$Z_{x2} = \frac{Z_{Lp} + jZ_1 \tan(2\theta)}{1 + jwC_r Z_{Lp} - wC_r Z_1 \tan(2\theta) + j\dfrac{Z_{Lp}}{Z_1}\tan(2\theta)} \tag{1c}$$

where $Z_{Lr} = (jw0.5C_r)^{-1}$ and $Z_{Lp} = (jw0.5C_p)^{-1}$ are the impedances of the reference and perturbation capacitances, respectively. Z_1 is the characteristic impedance of all uncoupled transmission lines. The coupled sections can also be expressed as [25]

$$Z_{11} = Z_{22} = Z_{33} = Z_{44} = \frac{-j}{2}(Z_{0e} + Z_{0o})\cot(\theta - \theta_a) \tag{2a}$$

$$Z_{12} = Z_{21} = Z_{34} = Z_{43} = \frac{-j}{2}(Z_{0e} - Z_{0o})\cot(\theta - \theta_a) \tag{2b}$$

$$Z_{13} = Z_{31} = Z_{24} = Z_{42} = \frac{-j}{2}(Z_{0e} - Z_{0o})\csc(\theta - \theta_a) \tag{2c}$$

$$Z_{14} = Z_{41} = Z_{23} = Z_{32} = \frac{-j}{2}(Z_{0e} + Z_{0o})\csc(\theta - \theta_a) \tag{2d}$$

Accordingly, input admittance of the even mode equivalent circuit can be expressed as

$$Y_{ine} = \frac{I_2}{V_2} + \frac{I_5}{V_5} = Y_{2x} + Y_{5x} \tag{3a}$$

where

$$Y_{2x} = \frac{A_2 Z_a}{A_2 Z_{13}^2 + A_2 Z_a Z_{11} - A_1 Z_a Z_{12} - A_1 Z_{13} Z_{14}} \tag{3b}$$

$$Y_{5x} = \frac{A_2 Z_b}{A_2 Z_b Z_{11} + A_2 Z_{13}^2 + A_1 Z_b Z_{12} + A_1 Z_{13} Z_{14}} \tag{3c}$$

with

$$A_1 = Z_{13}(Z_b - Z_a)(Z_{12}Z_{13} - Z_{11}Z_{14}) \tag{3d}$$

$$A_2 = 2Z_a Z_b\left(Z_{12}^2 - Z_{11}^2\right) + Z_{14}(Z_a + Z_b)(Z_{12}Z_{13} - Z_{11}Z_{14}) \tag{3e}$$

$$Z_a = -Z_{11} - Z_{in1} \tag{3f}$$

$$Z_b = -Z_{11} - Z_{in2} \tag{3g}$$

Input admittance of the odd mode equivalent circuit, Y_{ino}, can also be expressed from the analysis of Fig. 1*c*. Set of equations in (3a)–(3g) is also valid for the calculation of Y_{ino}. However, since the reference and perturbation capacitances in the symmetry axis are short-circuited, Z_{Lr} and Z_{Lp} must be taken as 0 in (1a)–(1c). From these equations, even and odd mode resonance conditions can be formulated as

$$\mathrm{Im}(Y_{ine}) = 0 \tag{4a}$$

$$\mathrm{Im}(Y_{ino}) = 0 \tag{4b}$$

The even and odd mode resonance frequencies can be tuned by changing the reference and perturbation capacitors. Since the perturbation capacitance is only placed in the even mode half circuit, it cannot affect the odd mode resonance frequency. In addition, S-parameters can be found as [25]

$$S_{11} = \frac{Y_0^2 - Y_{ine}Y_{ino}}{(Y_0 + Y_{ine})(Y_0 + Y_{ino})} \tag{5a}$$

$$S_{21} = \frac{Y_0(Y_{ino} - Y_{ine})}{(Y_0 + Y_{ine})(Y_0 + Y_{ino})} \tag{5b}$$

The frequencies at which the transmission zeros occur can also be found by

$$Y_{ino} - Y_{ine} = 0 \tag{6a}$$

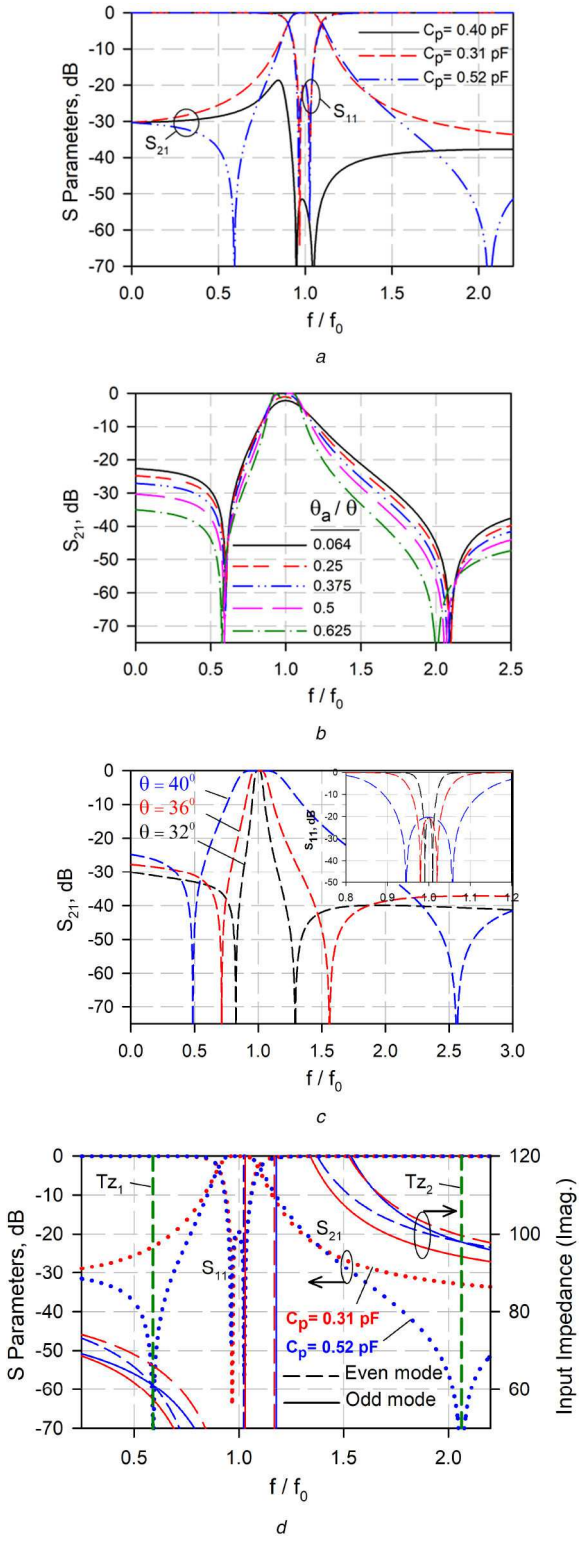

Fig. 2 *Normalised calculated frequency responses*
(a) Different filtering characteristics ($Z_{0e} = 97\,\Omega$, $Z_{0o} = 47\,\Omega$, $Z_1 = 75.4\,\Omega$, $Z_0 = 50\,\Omega$, $C_r = 0.4$ pF, $\theta = 40^0$, $\theta_a = 20^0$), ***(b)*** Different θ_a/θ rates ($C_r = 0.4$ pF, $C_p = 0.52$ pF, $\theta = 40^0$), ***(c)*** Different θ with $\theta_a = 10^0$, $C_r = 0.4$ pF and varied C_p at constant return loss level of 20 dB, ***(d)*** Representation of transmission zeros from input impedances

or

$$Z_{ine} - Z_{ino} = 0 \tag{6b}$$

In a DMSLR, the electrical length of θ must be different from 45^0 to obtain the transmission poles and zeros at finite frequencies. Fig. 2*a* depicts the normalised frequency responses for different filtering characteristics having two real-axis transmission zeros, two imaginary-axis transmission zeros and off states. It is clear that the real- and imaginary-axis transmission zeros can be obtained when C_p is smaller or greater than C_r, respectively. Moreover, there is no transmission observed, when C_p is equal to C_r. These are well-known characteristics of a conventional DMSLR [24]. In addition, the effects of θ_a/θ are demonstrated in Fig. 2*b*. Noted that the bandwidth and out-band insertion loss level can be adjusted depending on the ratio of θ_a/θ. It can be seen that the bandwidth of the filter also increases, as the electrical lengths of the coupled sections are increased. On the other hand, small shifts in the locations of the transmission zeros can be observed. Fig. 2*c* demonstrates the effects of different electrical lengths on the frequency response with fixed in-band return loss level of 20 dB. In order to keep this value at 20 dB, C_p must also be changed for each electrical length. Depending on the increment in θ, the bandwidth of the filter can be increased and locations of the transmission zeros exhibit more asymmetric behaviours. Moreover, input impedances under even and odd mode excitations are depicted in Fig. 2*d*. As can be seen from the figure, two frequency responses with respect to the existence of transmission zeros (Tz_1 and Tz_2) are represented. It is obvious that while the even and odd mode input impedances intersect, two transmission zeros can be observed.

2.2 Alternative coupling configurations

In the previous section, by considering symmetrically coupled sections, analysis of a DMSLR is realised by means of coupled line theory. However, in order to design multiplexer using DMSLRs, alternative coupling approaches should be taken into consideration to obtain deeper insertion loss levels in the upper stopband, so that isolation between the channels of the multiplexer can be increased. Depending on the equivalent circuit given in Fig. 1*a*, a tunable dual-mode filter can be arranged as shown in Fig. 3*a*. The layout of the filter is constructed on Rogers 4003C dielectric substrate with a relative dielectric constant of 3.38 and a thickness of 0.813 mm. By using variable capacitors instead of the reference and perturbation capacitors, it is possible to adjust the centre frequency of the filter according to (1a–c)–(3a–g). It should also be noted that each capacitor is connected to a patch element which can provide exact and easy tunability. Since the patch elements can behave as series capacitors, the values of the capacitors can be readily adjusted within the desired change range. Therefore, the total capacitance at each arm (C_r) in Fig. 1*a* will be the series sum of the variable capacitances and patch elements.

The effects of the asymmetric coupled sections on the frequency responses are investigated by changing the widths of feeding lines, w_f. Fig. 3*b* illustrates the behaviours of even/odd mode resonance frequencies and transmission zeros with respect to the changes in w_f. Although there are small shifts in even/odd mode resonance frequencies, locations of the transmission zeros are almost fixed. The effects of w_f on the FBW can also be observed from Fig. 3*b*. It can be seen that the FBW of the filter increases with respect to the change in w_f.

Moreover, since low out-band insertion loss may be needed in diplexer design, folded feeding lines are investigated as shown in Fig. 4. A dual-mode filter coupled to I/O ports with folded feeding lines is demonstrated in Fig. 4*a*. As can be seen from the figure, the electrical length of the feeding line is increased by the folded feeding configuration. Fig. 4*b* shows the effects of the folded feeding lines on the frequency response and it is investigated by comparing with the standard form given in Fig. 3*a*. Thus, deeper insertion loss at the upper stopband can be obtained. In this case, insertion loss level at the lower stopband may be obtained higher, and the lower transmission zero gets closer to the passband. The resonance occurred at 2.45 GHz in upper stopband is a disadvantage of this arrangement. It is resulted from the folded feeding line, which has an electrical length of $\lambda/2$ at the resonance frequency. However, in multiplexer designs, it can be tolerated by creating a transmission zero near the unwanted resonance. Also, the folded form can exhibit a filtering characteristic with only one

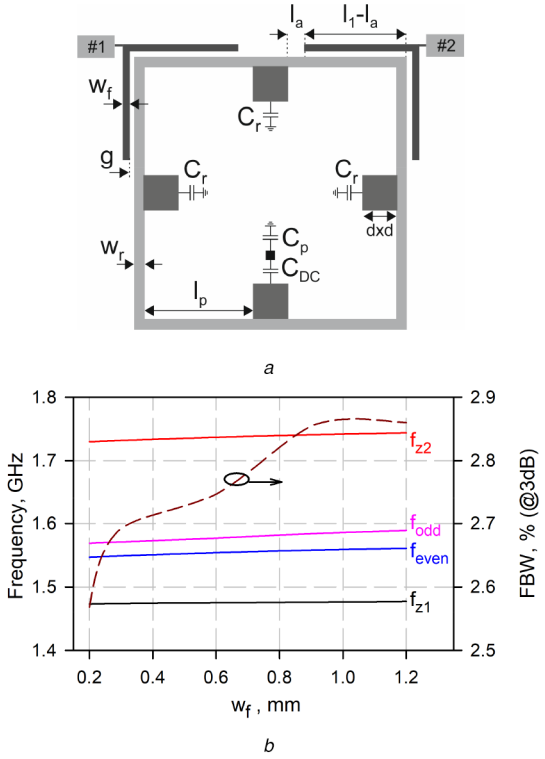

Fig. 3 *Dual-mode filter construction* ***(a)*** *A dual-mode filter coupled to I/O ports* ($C_r = 0.75$ pF, $C_p = 0.95$ pF, $C_{DC} = 8.2$ pF, $g = 0.15$ mm, $w_r = 0.9$ mm, $l_p = 9.2$ mm, $l_a = 0.65$ mm, $l_1 - l_a = 9.45$ mm, $d = 3$ mm), ***(b)*** *Effects of* w_f *on the transmission and reflection zeros*

transmission zero, while a filtering characteristic with two transmission zeros is obtained in the standard form. The behaviour of this transmission zero depending on the changes in C_r and C_p is shown in Fig. 4*c*. As can be seen from the figure, it is possible to change the location of the transmission zero. In addition, a right-side transmission zero can be observed when C_r is greater than C_p, and a left-side transmission zero can be observed when C_r is smaller than C_p.

3 Tunable and reconfigurable diplexer design

Based on the above analysis, a tunable microstrip diplexer can be designed by combining two DMSLRs having different electrical lengths. Depending on the desired diplexer response, they can be coupled to I/O ports by means of symmetric, asymmetric or folded feeding lines. For choosing the proper coupling configuration, the insertion loss and return loss levels of the channels, as well as, the isolation between the channels should be taken into consideration. Moreover, the final dimensions of the diplexer should be optimised to obtain proper tuning capabilities at each channel.

By using a matching circuit including the folded feeding lines and the asymmetric coupled line sections, a tunable microstrip diplexer is proposed as shown in Fig. 5. As can be seen from the figure, the patch element dimension of the upper resonator for the perturbation capacitor is different from the reference elements in order to achieve exact and proper tunability. The final dimensions are set by optimisations realised by using full-wave electromagnetic simulator, Sonnet [26]. Overall size of the designed diplexer is about 0.16 λ_g *x* 0.29 λ_g, where λ_g is the guided wavelength at the lowest centre frequency of the first channel. As can be seen from Fig. 5, the DMSLR for the second passband is coupled by only asymmetric feeding lines, while the other DMSLR for the first passband is coupled to I/O ports by folded and asymmetric feeding lines. Such a coupling structure is used to achieve an optimum isolation level between channels of the diplexer. In addition, the designed diplexer allows tuning filtering characteristics of each channel. In order to achieve tunability, the reference and perturbation capacitors in Fig. 1*a* are represented with varactor diodes, since they can provide variable capacitors.

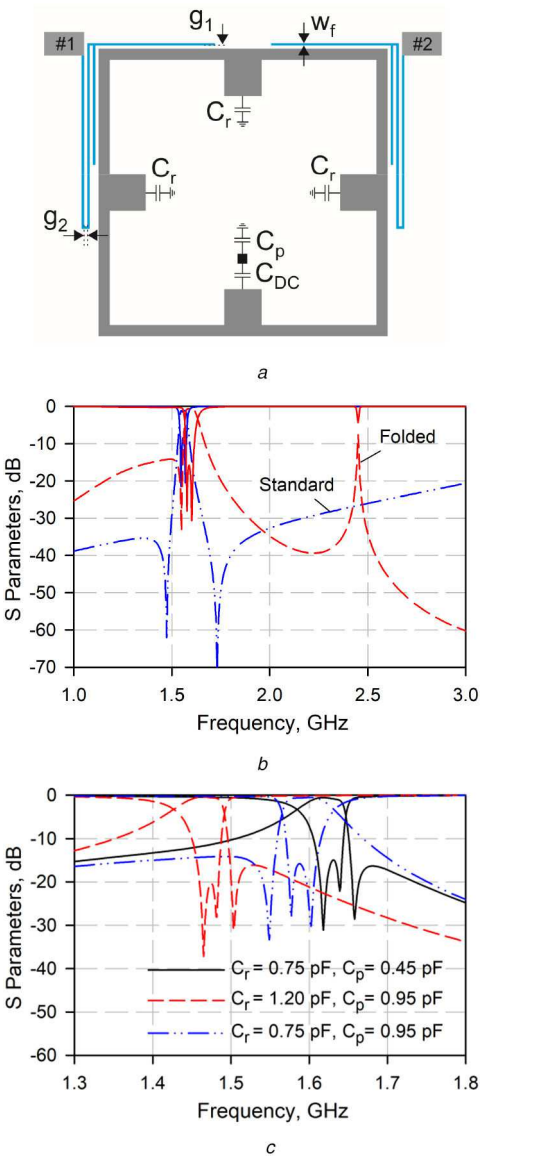

Fig. 4 *Investigations of the alternative feeding configurations*
(a) A dual-mode filter coupled to I/O ports with folded feeding lines ($w_f = 0.2$ mm, $g_1 = 0.15$ mm, $g_2 = 0.25$ mm), ***(b)*** Effects of folded feeding lines on the frequency response, ***(c)*** Behaviours of the transmission zeros with respect to the changes in C_r and C_p

For each resonator, to distinguish the effects of C_{p1} than that of C_{r1}, a DC block capacitor must be added between the perturbation varactor diode and the DMSLR. In this case, the reference varactor diodes can be simultaneously fed by a bias voltage on anywhere of the DMSLR, while the perturbation varactor diode is fed by a bias voltage between C_{p1} and C_{DC1}. In Fig. 5, total perturbation capacitance can be calculated by series summation of C_{p1}, C_{DC1} and the patch element (*pxp*), and total reference capacitances can be calculated by series summation of C_{r1} and the patch element (*dxd*). The varactor diodes are driven by DC bias voltages. While the first passband is tuned by V_1 and V_2, the second passband can be tuned by V_3 and V_4. It can also be seen that V_1 is the bias voltage of only C_{p1}, whereas V_2 is the bias voltage of all reference capacitors represented by C_{r1}. The same phenomenon is also valid for the other resonator in terms of V_3 and V_4. The effects of the varactor diode capacitances on the even and odd mode frequencies are depicted in Fig. 6. Fig. 6*a* shows the effects of C_{p1} and C_{r1} on the even and odd mode frequencies of the first channel. It is clear that C_{p1} can only tune the even mode frequency, whereas C_{r1} has effects on both of even and odd modes according to (4a) and (4b). Similar behaviours can also be obtained for the second channel as illustrated in Fig. 6*b*. On the other hand, coupling coefficients of

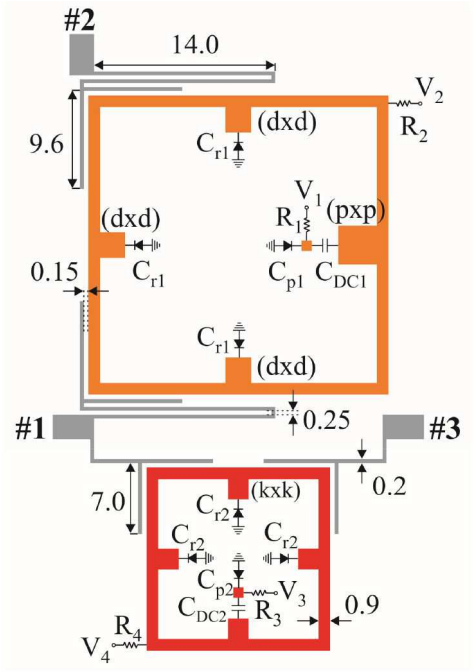

Fig. 5 *Proposed tunable microstrip diplexer* ($C_{DC1} = C_{DC2} = 8.2$ pF, $R_{1,2,3,4} = 10$ kΩ, $d = 3$ mm, $p = 4$ mm, $k = 1.6$ mm, *all dimensions in mm)*

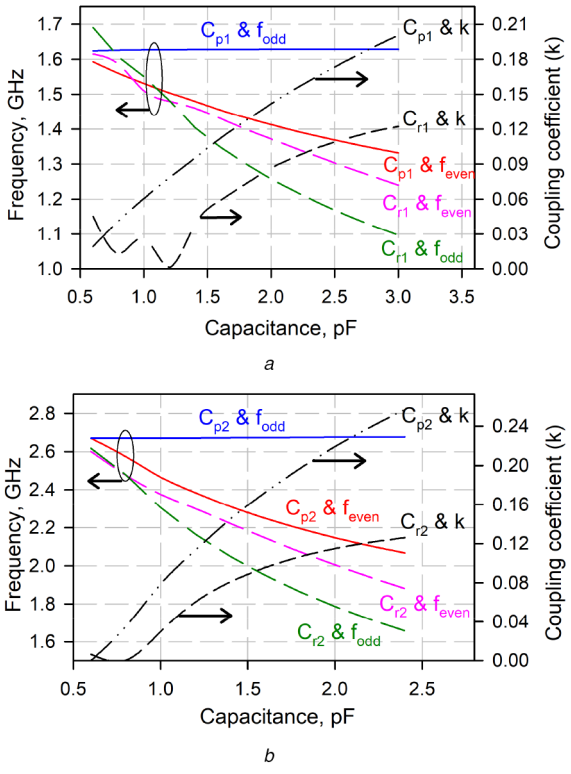

Fig. 6 *Mode frequencies and coupling coefficient investigations*
(a) First channel, ***(b)*** Second channel

the channels with respect to the changes in the reference and perturbation capacitances are also shown in Fig. 6. As is well known, the coupling coefficient between the even and odd mode frequencies of a DMSLR can be calculated as

$$k = \frac{2|f_e - f_o|}{f_e + f_o} \tag{7}$$

where f_e and f_o represent the even and odd mode frequencies, respectively. As can be seen from Fig. 6, the coupling coefficients

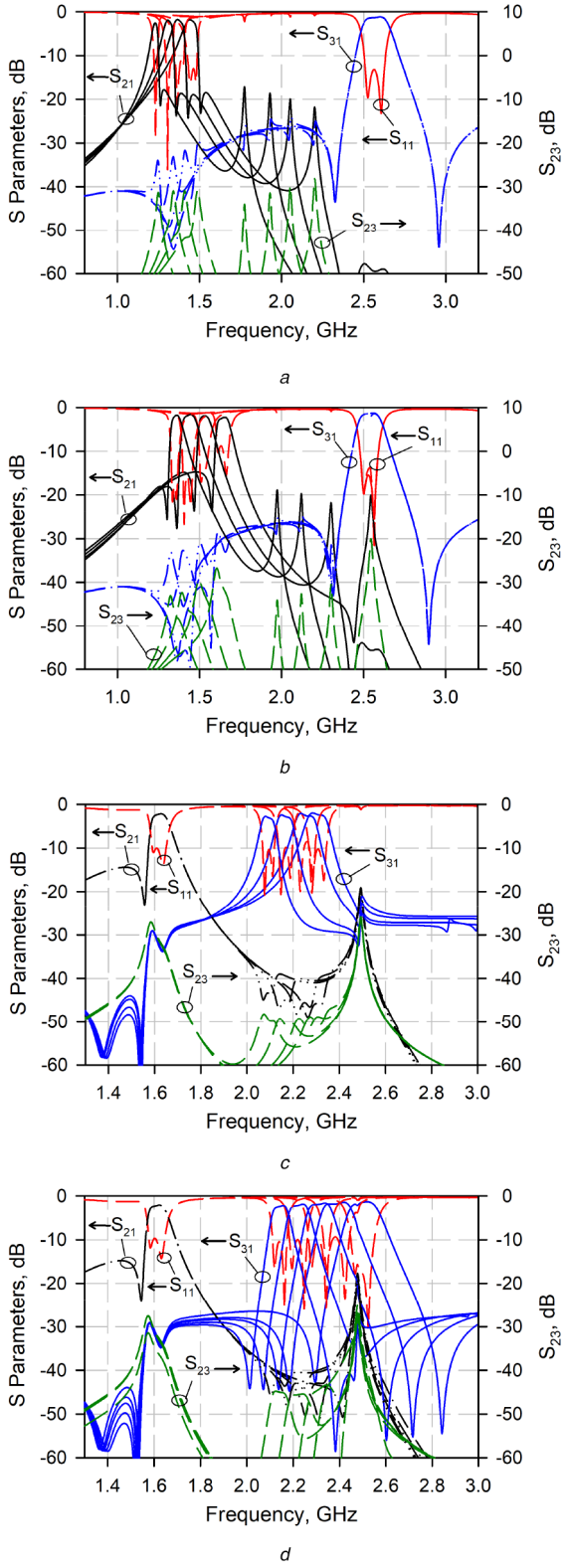

Fig. 7 *Simulated results*
(a) First channel with right-side transmission zero, ***(b)*** First channel with left-side transmission zero, ***(c)*** Second channel with two real-axis transmission zeros, ***(d)*** Second channel with two imaginary-axis transmission zeros

exhibit more stable behaviour for C_{p1} and C_{p2} as compared to C_{r1} and C_{r2}.

Simulated frequency responses for both channels are demonstrated in Fig. 7. In the simulations, the varactor diodes are utilised as ideal capacitors. The centre frequency tunability of the first channel is shown for filtering characteristics having the right- and left-side transmission zeros in Figs. 7*a* and *b*, respectively. As can be seen from Fig. 7*a*, there is only one transmission zero on the

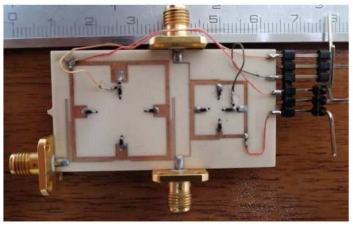

Fig. 8 *Photograph of the fabricated circuit*

right side of the passband. The centre frequency can be tuned between 1.23 and 1.44 GHz with a minimum insertion loss of 2.54 dB. The return loss and isolation levels are better than 10 and 28 dB, respectively. The FBWs are observed in the range of 3.1–6.19%. In this case C_{p1} and C_{r1} vary from 0.56 to 2.0 and 1.28 to 2.2 pF, respectively. Moreover, C_{p2} and C_{r2} are 0.85 and 0.62 pF, respectively.

As shown in Fig. 7*b*, there is only one transmission zero at the left side of the passband. The centre frequency can be tuned in a band of 1.36–1.65 GHz with a minimum insertion loss of 2.17 dB. The return loss and isolation between the output ports are better than 8.8 and 20 dB, respectively. FBWs over the tuning range are varied between 4.97 and 6.731%. In this tuning, C_{p1} and C_{r1} vary from 0.54 to 1.85 pF and 0.66 to 1.50 pF, respectively. Also, C_{p2} and C_{r2} are 0.87 and 0.66 pF, respectively.

The tunability for the second channel is illustrated in Figs. 7*c* and *d* according to the filtering characteristics with two real- and imaginary-axis transmission zeros, respectively. As can be seen from Fig. 7*c*, centre frequency of the second channel can be tuned between 2.09 and 2.3 GHz, with a minimum insertion loss of 2.74 dB. The return loss and isolation levels are better than 8.5 and 25 dB, respectively. FBWs for the depicted tuning range vary in the range of 3.16 and 4.48%. In this case, C_{p2} and C_{r2} vary from 0.83 to 1.24 pF and 1.03 to 1.35 pF, respectively. Also, C_{p1} and C_{r1} are 0.6 and 0.72 pF, respectively.

The tunability for the filtering characteristics with two imaginary-axis transmission zeros at the second channel is shown in Fig. 7*d*. The centre frequency can be tuned from 2.15 to 2.5 GHz with a minimum insertion loss of 2.18 dB. The return loss and isolation levels are better than 9.3 and 25 dB, respectively. The FBWs are within 3.73 and 6.03%. Also, C_{p2} and C_{r2} vary from 0.9 to 1.45 and 0.7 to 1.18 pF, respectively. During these tunings, C_{p1} and C_{r1} are fixed at 0.65 and 0.73 pF, respectively.

4 Experimental results

Designed tunable diplexer was fabricated and measured. Photograph of the fabricated circuit is shown in Fig. 8. The measurements were realised by using Keysight N5222A PNA Network Analyser. Infineon BB857 varactor diodes and AVX thin-film resistors and capacitors were used to represent the ideal circuit elements utilised in the simulations. The DC block capacitors and bias resistors have the same values with the simulations given in the previous section.

Measured results for both channels at different filtering characteristics are demonstrated in Fig. 9. Fig. 9*a* depicts the centre frequency tunability for the frequency response with right-side transmission zero. In this case, the tuning range was measured to be between 1.23 and 1.43 GHz with a minimum insertion loss of 5.82 dB. The minimum insertion loss varies within 3.09 and 5.82 dB. The return loss and isolation levels were measured to be better than 10 and 29 dB, respectively. For all cases, the FBWs are within 5.59 and 6.93%. V_1 and V_2 vary from 28.5 to 7.6 and 11.4 to 7.3 V, respectively.

As shown in Fig. 9*b*, the centre frequency of the first channel can be tuned between 1.35 and 1.64 GHz with a minimum insertion loss of 4.51 dB, and the transmission zero is located on the left side of the passband. The minimum insertion loss varies within 2.17 and 4.51 dB. The return loss and isolation levels were measured as better than 11 and 25 dB, respectively. FBWs over the tuning range were measured within 5.55 and 7.75%. V_1 and V_2 vary from 28.7 to

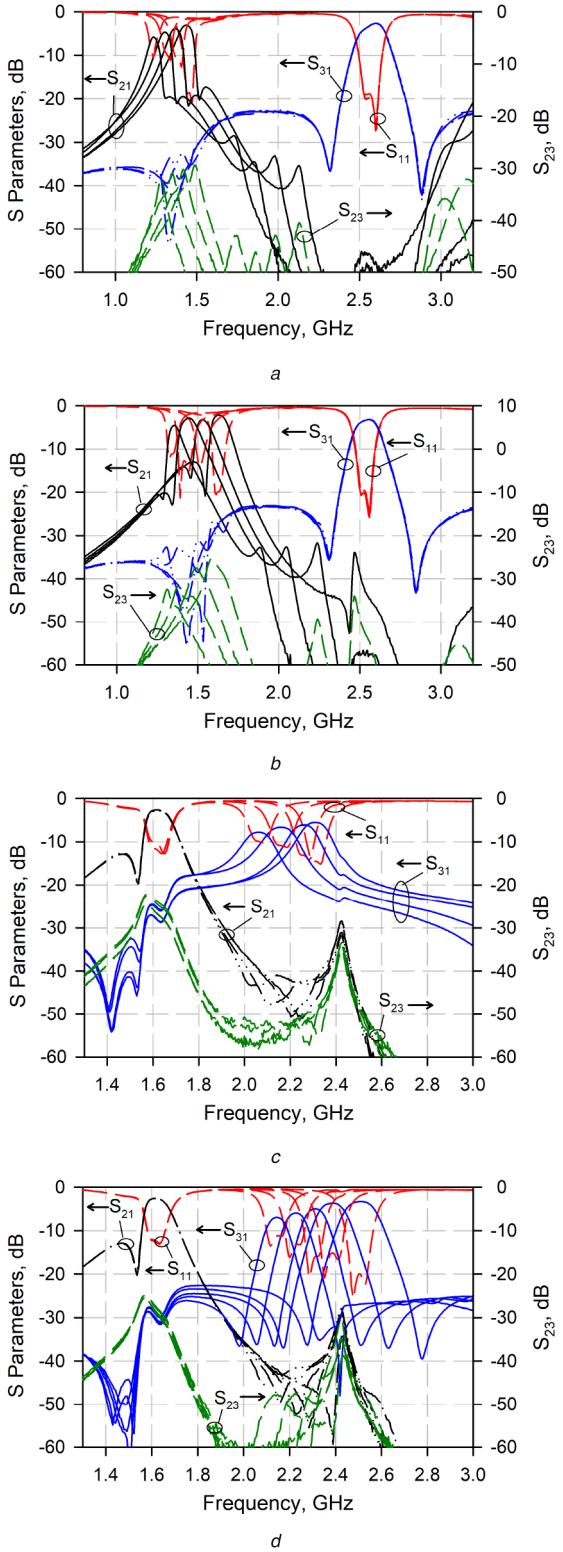

Fig. 9 *Measured results*
(a) First channel with right-side transmission zero, ***(b)*** First channel with left-side transmission zero, ***(c)*** Second channel with two real-axis transmission zeros, ***(d)*** Second channel with two imaginary-axis transmission zeros

8.2 and 26.8 to 9.5 V, respectively. The voltages V_3 and V_4 for the fixed second channel were nearly kept at 25 and 27 V, respectively.

For the second channel, centre frequency tunability of the filtering characteristics with two real-axis transmission zeros is shown in Fig. 9*c*. The tuning range was obtained between 2.07 and 2.31 GHz with a minimum insertion loss of 7.78 dB. The minimum insertion loss varies within 5.53 and 7.78 dB. The return loss and isolation levels are better than 9.7 and 22 dB, respectively. FBWs

Table 1 Comparisons with previous tunable diplexers

	TR, GHz	IL, dB	RL, dB	*I*, dB	$S\ (\lambda_g^2)$	RFC	FBW/ABW
[13]	0.71–0.92	1.5–3.2	>15	>22	0.027	–	7%
	1.0–1.2	1.6–3.5					6%
[14]	0.88–1.05	1.4–7.02	>15	>45	0.154	–	6.1± 0.4%
	1.66–1.87	3.42–6.7	>20				4±0.3% (3 dB)
[15]	1.42–2.07	6–7.7	>10	>20	0.036	–	∼4.8% (1 dB)
	1.53–2.27	5–7.68					
[16]	0.72–1.05	2.5–4	>15	>39	0.009	–	6.3–6.6%
	1.22–1.72	3–4.9					∼4.8% (1 dB)
[17]	0.755	0.8	NA	>24	0.0406	–	70±4 MHz (1 dB)
	1.05–1.21	1.12–2					
[18]	1.9–2.7	3.0–5.4	>10	>25	0.006 (λ_0^2)	–	6±0.3%
	2.5–3.4	3.5–6.3					4.5±0.3% (1 dB)
[19]	1.47–2.5	<2.5	>13	32	NA	–	247.5±26.5 MHz (3 dB)
	2.2–3.5	2.5–4.3					
[20]	1.05–1.35	<3.6	>10	>36	NA	–	133.5±2.5 MHz (3 dB)
	1.3–1.6	<3					
T.W. (A)	1.23–1.43	3.1–5.8	>10	>29	0.046	✓	5.6–6.9%
	2.07–2.31	5.5–7.8	>9.7	>22			5.9–7.1% (3 dB)
T.W. (B)	1.35–1.64	2.2–4.5	>11	>25			5.5–7.7%
	2.14–2.51	3.3–6.9	>11	>24			4.3–5.9% (3 dB)

IL: insertion loss, RL: return loss, TR: tuning range, *I*: isolation, *S*: Size, RFC: reconfigurable filtering characteristics, FBW/ABW: fractional bandwidth/absolute bandwidth, T.W. (A): right-side transmission zero for the first channel and the filtering characteristic with two real-axis transmission zeros for the second channel, T.W. (B): left-side transmission zero for the first channel and the filtering characteristic with two imaginary-axis transmission zeros for the second channel.

over the tuning range were measured within 5.90% and 7.01%. V_3 and V_4 vary from 25 to 14.5 V and 14 to 10.4 V, respectively.

For the frequency response with two imaginary-axis transmission zeros shown in Fig. 9*d*, the tuning range was measured between 2.14 and 2.51 GHz with a minimum insertion loss of 6.93 dB. The minimum insertion loss varies within 3.28 and 6.93 dB. The measured return loss and isolation levels were better than 11 and 24 dB, respectively. FBWs over the tuning range was measured within 4.34 and 5.99%. V_3 and V_4 vary from 20 to 12.5 and 22.5 to 13 V, respectively. The voltages V_1 and V_2 for the first channel were nearly fixed at 27 and 20 V, respectively.

It should be noted that the paper has focused on designing a tunable diplexer with reconfigurable filtering characteristics in some frequency bands of GPS and 4G-LTE technologies. Comparisons with tunable diplexers reported in the literature are given in Table 1. The designed diplexer allows changing the filtering characteristics at both channels electronically. This feature makes it more useful in the multifunction communication systems operating at different frequencies. It can be noted from the simulated and experimental results that the centre frequency of the first channel can be tuned for two filtering characteristics having left or right side transmission zero. Such reconfigurability can provide an advantage for the multifunction systems that need one-side selectivity. Depending on the coupling configuration, both of the transmission zeros for the second channel can be observed at real or imaginary frequencies. The centre frequency of the second channel can also be tuned independently. The tunable diplexer proposed in this work exhibits acceptable passband performances in both channels. Besides, in-band insertion loss levels can be improved by using varactor diodes having a lower loss.

5 Conclusion

A novel compact microstrip diplexer with tunable centre frequencies and reconfigurable filtering characteristics at both channels was designed by using DMSLRs. The design methodology was achieved by introducing the coupled line characteristics of a DMSLR. Tunability was realised by varactor diodes utilised instead of conventional perturbation and reference patch elements. Two DMSLRs having different electrical lengths were coupled to I/O ports by asymmetrical and folded feeding lines. Depending on the specialised values of the varactor diodes, both channels can be reconfigured by locating real- or imaginary-axis transmission zeros. By virtue of this approach, it is expected that the proposed tunable and reconfigurable structure can become advantageous for multifunction communication systems serving for GPS and 4G-LTE technologies. The designed diplexer was fabricated and tested to validate the theoretical and simulated results. The measured results are in good agreement with the simulated ones.

6 Acknowledgments

This work was supported by the Scientific and Technological Research Council of Turkey (TÜBİTAK) under Grant no. 215E099.

7 References

[1] Lo, W., Deng, P.H., Lin, C.H.: 'Microstrip diplexer and triplexer using mixed directed-feed and coupled-feed line coupled-resonator filters'. Progress in Electromagnetics Research Symp. - Fall (PIERS - FALL), Singapore, 2017, pp. 861–865

[2] Feng, W., Gao, X., Che, W.: 'Microstrip diplexer for GSM and WLAN bands using common shorted stubs', *IET Electron. Lett.*, 2014, **50**, (20), pp. 1486–1488

[3] Tantiviwat, S., Intarawiset, N., Jeenawong, R.: 'Wide-stopband, compact microstrip diplexer with common resonator using stepped-impedance resonators'. IEEE Tencon - Spring, Sydney, NSW, 2013, pp. 174–177

[4] Dhwaj, K., Jiang, L.J., Itoh, T.: 'Microstrip diplexer with low channel-frequency ratio'. Asia-Pacific Microwave Conf. (APMC), New Delhi, 2016, pp. 1–4

[5] Peng, H.S., Chiang, Y.C.: 'Microstrip diplexer constructed with new types of dual-mode ring filters', *IEEE Microw. Wirel. Compon. Lett.*, 2015, **25**, (1), pp. 7–9

[6] Gorur, A.K., Karpuz, C.: 'A novel microstrip triplexer based on meandered loop resonators'. IEEE Asia Pacific Microwave Conf., Kuala Lumpur, 2017, pp. 1242–1245

[7] Zhang, L., Wu, B., Qiu, F.: 'Compact six-band triplexer using stub-loaded stepped impedance resonators', *Electron. Lett.*, 2014, **50**, (16), pp. 1143–1145

[8] Lo, S., Hsu, K., Tu, W.: 'Compact and high-isolation microstrip quadruplexer'. Asia-Pacific Microwave Conf. Proc. (APMC), Seoul, 2013, pp. 966–968

[9] Tseng, B., Chang, S., Lin, C., *et al.*: 'A compact eight-channel microstrip quadruplexer using quad mode stub-load resonators'. 2014 Asia-Pacific Microwave Conf., Sendai, Japan, 2014, pp. 7–9

[10] Djoumessi, E.E., Wu, K.: 'Electronically tunable diplexer for frequency-agile transceiver front-end'. IEEE MTT-S Int. Microwave Symp., Anaheim, CA, 2010, pp. 1472–1475

[11] Chen, C., Tseng, B., Wang, G., *et al.*: 'Compact microstrip eight-channel multiplexer with independently switchable passbands', *IET Microw. Antennas Propag.*, 2018, **12**, (6), pp. 1026–1033

[12] Xu, J.: 'A tunable diplexer based on mixed coupling varactor-tuned stepped-impedance resonators', *Microw. Opt. Technol. Lett.*, 2016, **58**, (6), pp. 1469–1473
[13] Chen, C.F., Lin, C.-Y., Tseng, B.-H., *et al.*: 'A compact tunable microstrip diplexer using varactor-tuned dual-mode stub-loaded resonators'. IEEE MTT-S Int. Microwave Symp., Tampa, FL, 2014, pp. 1–3
[14] Feng, W., Zhang, Y., Che, W.: 'Tunable dual-band filter and diplexer based on folded open loop ring resonators', *IEEE Trans. Circuits Syst. II, Express Briefs*, 2017, **64**, (9), pp. 1047–1051
[15] Ko, C.H., Rebeiz, G.M.: 'A 1.4–2.3-GHz tunable diplexer based on reconfigurable matching networks', *IEEE Trans. Microw. Theory Tech.*, 2015, **63**, (5), pp. 1595–1602
[16] Gao, L., Lin, T., Rebeiz, G.M.: 'Design of tunable multi-pole multi-zero bandpass filters and diplexer with high selectivity and isolation', *IEEE Trans. Circuits Syst. I, Regul.Pap.*, 2019, **66**, (10), pp. 3831–3842
[17] Lu, Q., Zhang, Y., Cai, J., *et al.*: 'Microstrip tunable diplexer with separately-designable channels', *IEEE Trans. Circuits Syst. II, Express Briefs*, 2020, doi: 10.1109/TCSII.2020.2992273
[18] Yang, T., Rebeiz, G.M.: 'A simple and effective method for 1.9–3.4-GHz tunable diplexer with compact size and constant fractional bandwidth', *IEEE Trans. Microw. Theory Tech.*, 2016, **64**, (2), pp. 436–449
[19] Li, Z., Tang, X., Lu, D., *et al.*: 'Tunable diplexer with identical passband and constant absolute bandwidth', *IEEE Trans. Microw. Theory Tech.*, 2020, **68**, (2), pp. 721–731
[20] Lu, D., Yu, M., Barker, N.S., *et al.*: 'Advanced synthesis of wide-tuning-range frequency-adaptive bandpass filter with constant absolute bandwidth', *IEEE Trans. Microw. Theory Tech.*, 2019, **67**, (11), pp. 4362–4375
[21] Khan, A.A., Mandal, M.K.: 'Design of planar diplexers with improved isolation using the tunable transmission zeros of a dual-mode cavity filter', *IET Microw. Antennas Propag.*, 2017, **11**, (11), pp. 1587–1593
[22] Liu, X., Tian, Z., Qian, H.J., *et al.*: 'Reconfigurable diplexer using λ/2 resonator with hybrid varactor-embedded stepped-impedance open-stub and slot'. IEEE MTT-S Int. Wireless Symp., Chengdu, 2018, p. 1–4
[23] Karpuz, C., Gorur, A.K., Basmaci, A.N.: 'Design of tunable microstrip dual-mode bandpass filter having reconfigurable filtering characteristics for mobile applications'. European Microwave Conf., London, 2016, pp. 647–650
[24] Gorur, A.: 'Description of coupling between degenerate modes of a dual-mode microstrip loop resonator using a novel perturbation arrangement and its dual-mode bandpass filter applications', *IEEE Trans. Microw. Theory Tech.*, 2004, **52**, (2), pp. 671–677
[25] Pozar, D.M.: '*Microwave engineering*' (Wiley, New York, NY, USA, 2003, 3rd edn.), pp. 341–345
[26] Sonnet 16.52 User's Manuals: North Syracuse, NY, Sonnet Software, Inc., 2015